NAUKI PODSTAWOWE
CZASOPISMO TECHNICZNE
TECHNICAL TRANSACTIONS
FUNDAMENTAL SCIENCES
WYDAWNICTWO POLITECHNIKI KRAKOWSKIEJ
1-NP/2009
ZESZYT 8
ROK 106
ISSUE 8
YEAR 106

WIESŁAWA BAŻELA*, WŁODZIMIERZ DYAKONOV**, MARCIN DUL*

X-RAY DIFFRACTION AND MAGNETIC PROPERTIES MEASUREMENT OF NANOPOWDER $(La_{0.7}Sr_{0.3})_{0.9}Mn_{1.1}O_3$ MANGANITE

RENTGENOWSKA DYFRAKTOMETRIA I POMIARY MAGNETYCZNE NANOPROSZKOWEGO MANGANITU $(La_{0.7}Sr_{0.3})_{0.9}Mn_{1.1}O_3$

Abstract

We report on the X-ray powder diffraction and magnetic measurements of nanosize $(La_{0.7}Sr_{0.3})_{0.9}Mn_{1.1}O_3$ manganite. The nanoparticles were synthesized with use of co-precipitation method at different (800, 900 and 950°C) temperatures. Their crystal structure was determined to be perovskite-like with a rhombohedral distortion (the space group $R\ \bar{3}c$). The phase composition and specific surface nanopowders were determined. The average size of synthesized nanoparticles (from 32 to 88 nm) was estimated by both the method of low temperature adsorption of argon and X-ray diffraction measurements. All the nanosize samples show ferromagnetic-like ordering with close phase transition temperatures. Their magnetization decreases with reducing the particle size. The decrease of magnetization with decreasing particle size is due to increasing the surface contribution to magnetization. The magnetic entropy was shown to increase with increasing applied magnetic field and to be smaller for the small particles.

Keywords: *nanostructures, manganite, X-ray diffraction, magnetic measurement*

Streszczenie

W artykule przedstawiono wyniki pomiarów dyfrakcji rentgenowskiej oraz uzyskanych metodą magnetometryczną nanorozmiarowego manganitu $(La_{0.7}Sr_{0.3})_{0.9}Mn_{1.1}O_3$. Próbki otrzymano metodą zol–żel w następujących temperaturach: 800, 900 i 950°C. Wszystkie próbki krystalizują w układzie romboedrycznym (grupa przestrzenna $R\ \bar{3}c$). Średni rozmiar ziaren (od 32 do 88 nm) określono za pomocą rentgenowskiej dyfrakcji proszkowej oraz metodą niskotemperaturowej adsorpcji argonu. Wszystkie próbki wykazują ferromagnetyczne uporządkowanie z bliskimi temperaturami przejścia fazowego i ich namagnesowanie maleje wraz ze zmniejszaniem się rozmiarów ziaren. Zmniejszenie namagnesowania wraz ze zwiększaniem się rozmiarów ziaren jest spowodowane wzrostem wkładu powierzchni ziaren do namagnesowania. Magnetyczna entropia rośnie wraz ze wzrostem pola magnetycznego i jest mniejsza dla małych ziaren.

Słowa kluczowe: *nanostruktury, manganity, dyfrakcja rentgenowska, pomiary magnetyczne*

* Dr hab. Wiesława Bażela, mgr inż. Marcin Dul, Instytut Fizyki, Wydział Fizyki, Matematyki i Informatyki Stosowanej, Politechnika Krakowska.
** Prof. dr hab. Włodzimierz Dyakonov, Instytut Fizyki, Polska Akademia Nauk, Warszawa.

1. Introduction

At present, the most interesting metal-oxide materials are rare-earth manganites with the chemical composition of $(RE_{1-x}M_x)_yMn_{1+y}O_3$, where RE = La, Pr, Nd, and M = Sr, Ca, Ba, manifesting the colossal magnetoresistive (CMR) effect [1–3]. Their studies were performed mainly on bulk materials (ceramic, single crystals) and thin films. Physical properties of mixed valent perovskite manganites were shown to depend crucially on both doping level and the nature of doping element as well as on various intrinsic inhomogeneities among which the nanostructure deserves the special attention. Due to small size, these nanocrystallites exhibit novel properties which are significantly different from those of the bulk material. One important factor is increasing surface to volume of the grains ratio as the particle sizes reduce to the nanoscale. As a result, the small-size effect and surface effect perturb the structure and properties of nanoparticles. The intensive discussions devoted to synthesis, characterization of nanosized manganites, study the influence of grain size down to nanometric dimensions on the magnetism and transport of manganites as well as their application are present in the Refs. [4–16]. *dc* magnetization measurements of nanosize (the average particles size of 35 nm) $La_{0.3}Ca_{0.7}MnO_3$ manganite did not show significant change of the magnetic phase transition temperature in respect to its bulk counterpart [4]. The magnetization measurements of $La_{5/8-0.3}Pr_{0.3}Ca_{3/8}MnO_3$ (LPCMO) manganite under pressure up to 9.5 kbar have shown that pressure effect on ferromagnetic ordering in nanopowder (the grain sizes from 40 to 1000 nm) LPCMO is similar to that obtained for bulk samples [5]. An applied pressure enhances the phase transition temperature of $La_{1-x}MnO_{3+d}$ particles (20–30 nm) with a pressure coefficient of $dT_C/dP \approx$ $\approx$ 1.4 – 1.9 $kbar^{-1}$ [6]. The 30 nm nanoparticles of $La_{0.7}Sr_{0.3}MnO_3$ (LSMO) also exhibit the Curie temperature close to stoichiometric phase-pure LSMO [7]. A reduction of grain size in the $La_{0.7}Sr_{0.3}MnO_3$ [8] and $La_{2/3}Ca_{1/3}MnO_3$ [9] compounds was found to decrease magnetization due to increasing ratio of surface to volume of the grains. The grain size (from 53 to 8 nm) induced variations in structural and magnetic properties observed in $La_{0.8}Sr_{0.2}MnO_3$ nano-ferromagnet indicate a very important role of the particle surface effects [10]. The temperature dependences of magnetization of $La_{0.8}Sr_{0.2}MnO_3$ show that the nanoparticles with the grain size below 25 nm exhibit superparamagnetic behavior. Magnetic resonance spectra have been studied to obtain microscopic information on the magnetic structure of nanosize $La_{0.7}Sr_{0.3}MnO_3$ [11, 12].

The particle size effect on the electron transport of manganites have been also investigated [8, 13–16]. A magnetoresistance above 10% was obtained in a field of 1 kOe for all the particles sizes (from 20 to 110 nm) of $La_{0.67}Ca_{0.33}MnO_3$ [8]. Both the resistivity and high-field magnetoresistance of $La_{2/3}Sr_{1/3}MnO_3$ manganite having the grain diameters ranging from 10 μm to 20 nm increase substantially as the particle size decreases, while the maximum magnetoresistance exhibited by the nanosize powders near the Curie temperature is found to be not sensitive to the particle size [13, 14]. Unlike the bulk manganites, in nanostructured manganites a low field magnetoresistance was observed. The ultrafine (18 nm) $La_{2/3}Ca_{1/3}MnO_3$ powder is insulating from 5 to 300 K and is superparamagnetic above the blocking temperature corresponding to the peak in the ZFC magnetization [15]. When the temperature is below blocking temperature, the magnetoresistance is shown to be associated with the spin-polarized tunneling between grains. In Ref. [16], a model for the nanoparticles based on the existence of a noncollinear,

amorphous surface layer at the grains was supposed to explain both the higher resistivity and the reduction of saturation magnetization in the smaller particle samples. It should be noted that a clear understanding of the magnetic and transport properties caused by nanostructuration of manganite is still lacking.

In this paper, we report on the synthesis and characterization of nanopowder $(La_{0.7}Sr_{0.3})_{0.9}Mn_{1.1}O_3$ manganites as well as on the study of influence of the nanostructure on shape of X-ray pattern and their magnetic properties.

The manganese-lanthanum-strontium manganite $(La_{0.7}Sr_{0.3})_{0.9}Mn_{1.1}O_3$ with high phase transition temperature (about of 360 K) has been studied. Since the excess manganese increases MRE [17], this compound is perspective for application in the high sensitive sensor of magnetic field [18, 19]. A large magnetic moment at room temperature allows to use the nanoparticles of this manganite coated with appropriate makromolecules for application in biomedical diagnostic [20].

The format of the paper is as a follows. In Introduction, the analysis of papers devoted to the influence of grain size down to nanometric dimensions on the magnetic and transport properties manganites is presented.

In the first section, the brief information on the main experimental details, namely, nanosize samples preparation, crystalline structure, X-ray powder diffraction and magnetization measurements, are reported. The experimental methods have allowed to obtain information on the particle size effect on a physical properties as well as on peculiarities of behavior of nanopowder $(La_{0.7}Sr_{0.3})_{0.9}Mn_{1.1}O_3$ manganite studied.

The grain size effect on magnetic properties is presented in the second section. Based on the experimental results, the magnetic moment is shown to depend strongly on the average particles size, $< d >$, while both the magnetic phase transition temperature and the paramagnetic Curie–Weiss temperature change insignificantly with varying $< d >$. There is a tendency towards a decrease of both magnetic moment and magnetic entropy with decreasing $< d >$.

The summary suggests that the nanostructuration of the grains plays an important role in the formation of magnetic properties.

2. Sample and experimental

The methods of preparation of manganite nanoparticles are non-trivial. In this work, the co-precipitation technology of production of nanosize stochiometric manganese--lanthanum-strontium perovskites has been used. The mixture of stoichiometric amounts of high purity Mn_3O_4, La_2O_3 and $SrCO_3$ powders was dissolved in diluted nitric acid. This solution was evaporated to dryness, and then, it was fired at 500°C to decompose the nitrates. Dry remainder was thoroughly grinded and again was annealed at different (800, 900 and 950°C) for duration of 20 h in air, followed by a slow cooling down to T_{room}. The resulting material was repeatedly grinded, and the nanopowder with the average particle size of 32, 67 and 88 nm was obtained. The chemical composition of these powders checked with room temperature X-ray diffraction method is close to molar one of $(La_{0.6}Sr_{0.3})_{0.9}Mn_{1.1}O_3$. The oxygen content was determined by the gravimetric and iodometric methods.

The crystallographic structure and lattice parameters of the nanoparticle samples were determined with room temperature X-ray powder diffraction (XRD). XRD patterns were recorded on Philips PW-3710 X'PERT diffractometer using CuKα radiation. The 2θ scan are performed with the steps of 0.01 and counting time of 5 s step. The data were analyzed with the Rietveld-type refinement softwere FullProf program [21]. Comparison of experimental X-ray patterns of nanosize samples studied with different grain sizes is shown in Fig. 1a). XRD pattern for the sample with 800°C annealing temperature

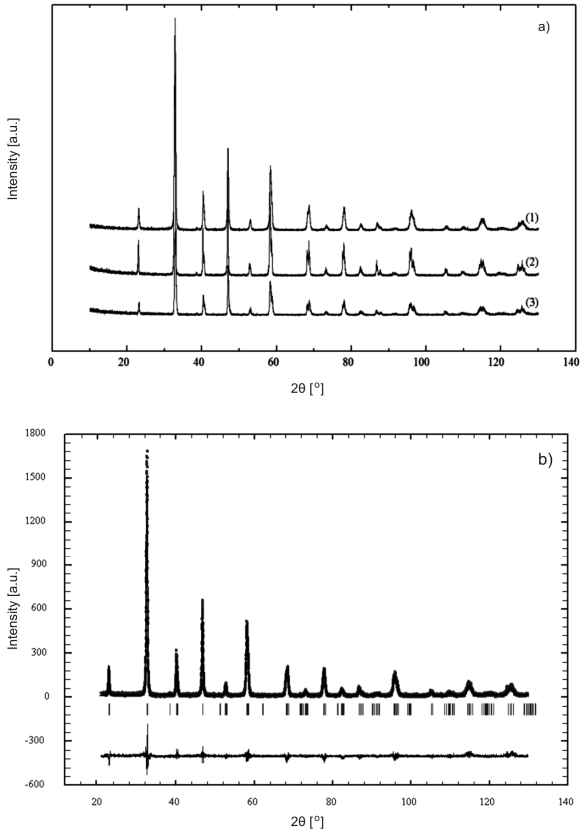

Fig. 1. (a) Experimental X-ray patterns for the samples of $(La_{0.7}Sr_{0.3})_{0.9}Mn_{1.1}O_3$ with 950 (1), 900 (2) and 800°C (3) annealing temperatures; (b) XRD pattern for the sample with 800°C annealing temperature together with Rietveld fit and difference plot. The vertical bars indicate the positions of Bragg reflections

Rys. 1. (a) Widma dyfrakcyjne dla próbek związku $(La_{0.7}Sr_{0.3})_{0.9}Mn_{1.1}O_3$ otrzymanych w następujących temperaturach: 950 (1), 900 (2) i 800°C (3); (b) dyfraktogram dla próbki wygrzewanej w temperaturze 800°C z uwzględnieniem dopasowania metodą Rietvelda oraz różnica między eksperymentem a modelem struktury. Pionowe kreski wskazują położenie refleksów braggowskich

is presented in Fig. 1b). The cross points are the actual data and the calculated curve is superposed on it. The short bars are the calculated positions of the reflections for

rhombohedral compounds. The bottom line showing the difference between the experimental and calculated XRD patterns indicate a good agreement between the observed and calculated intensities.

The X-ray diffraction data indicate that the samples obtained by annealing at $T > 800°C$ are homogeneous single phase compounds and their crystal structure is perovskite-like with a rhombohedral distortion (the space group $R\ \bar{3}c$). The atoms occupy the following positions: (La, Sr) in the 2a site (1/4, 1/4, 1/4); Mn in the 2b – (0, 0, 0) and O in 6e – (x,1/2–x,1/4). The crystal structure parameters determined are present in Table 1. The change of particle size was seen to produce an insignificant increase of the *a* lattice parameter and an insignificant deviation of the α edge from 60°.

The grain size of nanopowders obtained by the above-mentioned method was estimated by both the method of low temperature adsorption of argon and X-ray diffraction measurement. The method of low temperature adsorption of argon known as BET's method [22] has allowed to determine the specific surface (S_{SS}). The average particles sizes $< d >$ were calculated using the expression $S_{SS} = 1/(< d > \sigma_\gamma)$ and knowing the X-ray density $\sigma_\gamma = m_{e.c.}/(a/2)^3$, where $m_{e.c}$ is the mass elementary cell and *a* is the lattice parameter.

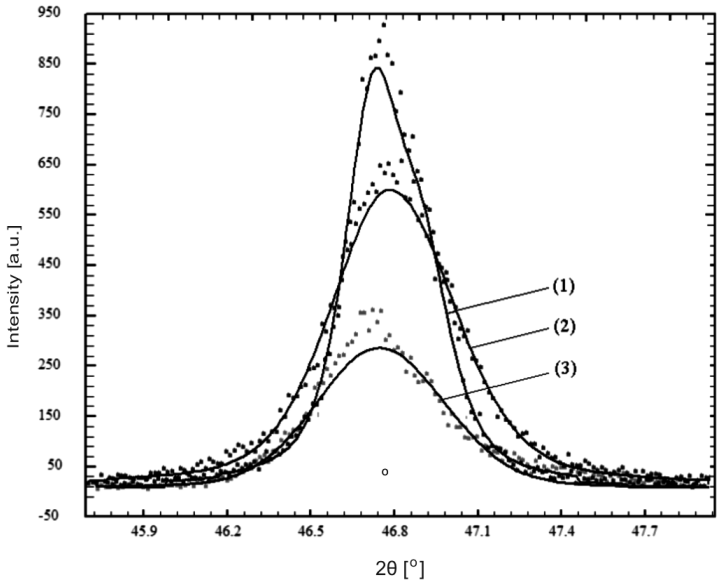

Fig. 2. Broadening of the (024) line profiles of the diffraction pattern as a result of decrease of the grain size (curves 1, 2 and 3 related to the samples with grain sizes of 88, 67 and 32 nm, respectively)
Rys. 2. Poszerzenie refleksu braggowskiego (024) jako rezultat zmniejszenia rozmiaru ziaren (krzywe 1, 2 i 3 odpowiadają próbkom o rozmiarach ziaren 88, 67 i 32 nm)

X-ray diffraction analysis has been carried out after each annealing step. Analysis of both the full XRD patterns and individual reflections reveals that the reflex profiles broaden out as the particles size goes down (Fig. 2). The grains sizes were determined using the Scherrer relation $d = \lambda/B \cos\theta$ [23]. Here *d* is the grain size, $\lambda = 1.54178$ Å

the X-rays wavelength, θ the corresponding angle of Bragg diffraction and *B* the difference between half-widths of the Bragg reflex of the nanopowder and the standard sample. The standard sample of Si powder with the size 10 micrometer [24] was used to calibrate the intrinsic width associated to the equipment. The (024) reflection of the diffraction pattern was used to calculate the particle size. Figure 2 shows a broadening of the (024) line profiles as a result of decrease of the grain size. The average grain sizes calculated by BET's method and obtained from XRD are close to each other (Table 1).

Table 1

Physical and chemical characteristics of nanopowders prepared at temperatures of 950 (S1), 900 (S2) and 800°C (S3)

Sample	Lattice parameters		Specific surface	Density	Particle size from XRD	Particle size from S_{SS}
	a [Å]	α [°]	S_{SS} [m^2/g]	σ_γ [g/cm^3]	$< d >$ [nm]	$< d >$ [nm]
S1	5.465	60.38	1.7	5.891	88	100
S2	5.467	60.37	2.3	5.893	67	75
S3	5.470	60.35	5.8	5.805	32	40

As it is seen in Table 1, the nanopowders obtained essentially differ by both a specific surface value and the average grains size. The average size of nanoparticles is within the range of about 32–88 nm.

The magnetization measurements were performed with a vibrating sample magnetometer in the temperature range of 5–375 K and in magnetic fields from 0.05 T to 1 T. Both zero-field-cooled (ZFC) and field-cooled (FC) magnetization vs. temperature and at selected magnetic field were measured.

For magnetic measurements, the nanopowders obtained were pressed at room temperature under pressure of 0.2 GPa into pellets 1.5 mm thick and 6 mm in diameter.

3. Results and discussion

In this paper, the experimental and theoretical studies of magnetism and transport in the $(La_{0.7}Sr_{0.3})_{0.9}Mn_{1.1}O_3$ manganites with the nanoparticle sizes of $< d > = 88$ (S1), 67 (S2) and 32 (S3) nm are presented. According to room temperature X-ray diffraction (XRD) measurements the nanoparticle samples are homogeneous single phase compounds. Their crystal structure was determined to be perovskite-like with a rhombohedral distortion (the space group $R\,\bar{3}c$). The change of particle size from 88 to 32 nm was established to produce an insignificant increase of the *a* lattice parameter and an insignificant deviation of the α edge from 60° (Table 1).

3.1. Magnetic properties

3.1.1. *dc* magnetization

The temperature variation of *dc* magnetization for three nanopowders under consideration in magnetic field of 0.05 T near the phase transition is depicted in Fig. 3.

For all samples, the ferromagnetic-like behavior is observed. Near the phase transition temperature, the magnetization begins to rise sharply with decreasing temperature indicating the onset of ferromagnetic ordering and tends to the saturation. It is seen that the magnetization is strongly influenced by the particles size and decreases as the grain size of the particles diminishes. In inset to Fig. 3, the $M_{FC}(T)$ dependences for the S3 sample in magnetic fields of 0.05–0.5 T are shown. The influence of magnetic field on the $M_{FC}(T)$ dependences for the another samples is similar.

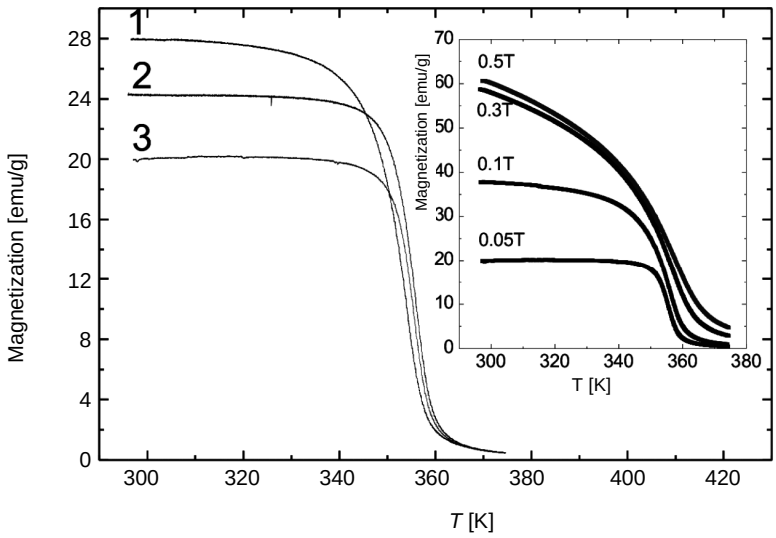

Fig. 3. Temperature variation of magnetization for the S1, S2 and S3 (curves 1–3, respectively) nanopowders under consideration in magnetic field of 0.05 T. Inset: $M_{FC}(T)$ dependences for the S3 sample in magnetic fields of 0.05–0.5 T

Rys. 3. Temperaturowa zmiana namagnesowania dla próbek S1, S2 i S3 (odpowiednio: krzywe 1–3) w polu magnetycznym 0,05 T. Wstawka: Zależności $M_{FC}(T)$ dla próbki S3 w polach magnetycznych 0,05–0,5 T

The low temperature field cooled (M_{FC}) and zero field cooled (M_{ZFC}) magnetization recorded in magnetic field of 0.1 T for all samples are presented in Fig. 4a).

Figure 4b) shows the FC and ZFC magnetization for S1 and S2 as a function of temperature near phase transition. The insignificant difference between FC and ZFC magnetization, which begins to diverge below 340, 300 and 275 K for S1, S2 and S3, respectively, and increases with decreasing temperature, indicates the presence of a small magnetic anisotropy. The difference between M_{ZFC} and M_{FC} magnetization diminishes in magnetic field and disappears between 0.1 and 0.3 T. The local maximum observed in the magnetization curves at low temperatures (about 42 K) suggests a possible frustration effect induced by a competition from different magnetic interactions, that can result in spin canting at lower temperature due to an excess manganese [17]. This fact could be consist with an antiferromagnetic ordering in Mn^{3+}–O–Mn^{4+} clusters [25].

The analysis of high-temperature *dc* susceptibilities, (M/H), of samples studied was performed using the Curie–Weiss (CW) law

$$\chi(T) = \chi_0 + \frac{C}{T - \theta} \tag{1}$$

where χ_0 is the background susceptibility, the Curie constant $C = \frac{1}{7k_s}\mu_{\text{eff}}^2$, $\mu_{\text{eff}}(S) = \mu_B g\sqrt{S(S+1)}$ the effective magnetic moment, θ the paramagnetic CW temperature.

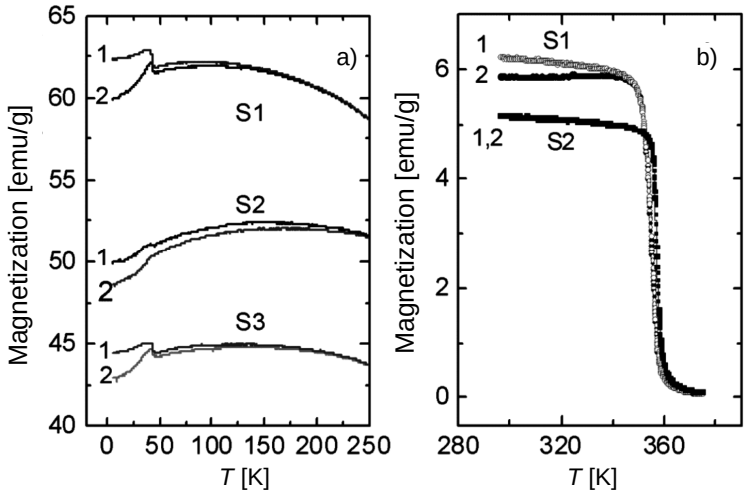

Fig. 4. Temperature dependence of field cooled (M_{FC}) (curve 1) and zero field cooled (M_{ZFC}) (curve 2) magnetization recorded in magnetic field of 0.1 T for S1, S2, S3 samples (a). The FC and ZFC magnetization (curves 1 and 2, respectively) as a function of temperature for S1 and S2 in field of 0.01 T (b)

Rys. 4. Temperaturowe zależności namagnesowania mierzone w polu (M_{FC}) (krzywa 1) i bez pola (M_{ZFC}) (krzywa 2) otrzymane w polu magnetycznym 0,1 T dla próbek S1, S2 i S3 (a). Namagnesowanie FC i ZFC (odpowiednio: krzywe 1 i 2) jako funkcja temperatury dla próbek S1 i S2 w polu magnetycznym 0,01 T (b)

The experimental $H/M(T)$ dependences for samples S2 in fields of H = 0.05, 0.1, 0.3 and 0.5 T are presented in Fig. 5, respectively.

Similar $H/M(T)$ dependences were obtained for the another samples. The fitting of the experimental $M(T)$ dependences to the CW law (1) has shown that $H/M(T)$ curves as a function of temperature are linear at temperatures above T_C and obey the CW law for all samples. A root-mean square error of fitting is equal to ≈ 0.2%. The Curie temperatures, θ, calculated as a result of a fitting of CW law to the experimental data were found to have the positive sign that is indicative of dominant ferromagnetic interactions. The θ temperatures do not depend practically on changes of $< d >$. Using the CW constant values the effective numbers of Bohr magneton, n_{eff}, were calculated. The χ_0, C, θ, T_C, n_{eff} values of as a function of $< d >$ are summarized in Table 2. In magnetic fields from 0.1 to 0.5 T, the χ_0, C and n_{eff} parameters calculated decrease insignificantly.

The theoretical estimation of the effective magnetic moment in nano-size manganites is of interest. In systems with variable valency of ions Mn^{3+} (concentration x) and Mn^{4+} (concentration $1 - x$), the total magnetic moment μ_{tot} can be written in the form

$$\mu_{tot}^2 = x\mu_{eff}^2(S_1) + (1-x)\mu_{eff}^2(S_2) \tag{2}$$

where $S_1 = 2$ and $S_2 = 3/2$ are the spins of Mn^{3+} and Mn^{4+} ions, respectively, $x = 0.7$ is the Mn^{3+} concentration and g-factor is equal to 2. The high value of the total moment equal to $\mu_{tot} = 4.62\ \mu_B$ was obtained. The μ_{tot} value is between the spin-only values for Mn^{3+} ($4.9\ \mu_B$) and Mn^{4+} ($3.87\ \mu_B$) ions. In our case, the effective number of Bohr magnetons determined experimentally are higher than the total effective moment value calculated. Similar situation was observed in Ref. [26], where for the system $La_{0.93}MnO_3$ with Mn^{4+} concentration $1 - x = 0.21$ the experimental and calculated values of the total effective moment are equal to 4.7 and 5.8 μ_B, respectively. It was concluded that in a paramagnetic phase the polaron effects are responsible for formation of the magnetic clusters. As the result, it leads to increase of Curie constants and, respectively, to increase of the total effective magnetic moment.

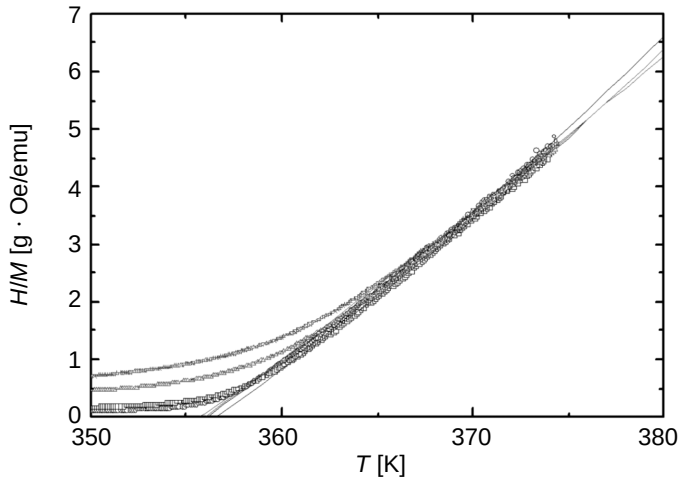

Fig. 5. Experimental $H/M(T)$ dependences for S2 sample in fields of H = 0.05, 0.1, 0.3 and 0.5 T (fitting of the experimental $M(T)$ dependences to the Curie–Weiss law is shown by solid line)

Rys. 5. Temperaturowe zależności $H/M(T)$ dla próbki S2 w polach H = 0,05, 0,1, 0,3 i 0,5 T (dopasowanie eksperymentalnych zależności $M(T)$ do prawa Curie–Weiss jest zaznaczone linią ciągłą)

The FM phase transition temperatures (T_C) were defined from peak of dM/dT in the $M(T)$ dependence. Despite the particle size difference, the Curie temperatures were found to coincide practically (±2 K) for all samples studied (Table 2). This means that the inner parts (cores) of grains in all nanopowders are magnetically identical, i.e. a Mn^{3+}/Mn^{4+} ratio in the nanoparticles is similar, and their contribution to the magnetization is nearly the same. It agrees with a model of the nanoparticles presented in [16].

The T_C temperatures determined are close to those in a bulk manganite of the same composition.

Additional information on the magnetic properties was obtained by the measurements of both the $M(T)$ magnetization in applied magnetic field and $M(H)$ isotherms. The magnetization is highly dependent on the applied magnetic field (Inset to Fig. 3). The paramagnet-ferromagnet phase transition in magnetic field becomes broader and the $M(T)$ dependence shifts towards high temperatures what indicates a extension of the FM phase. Figure 6 shows a comparison of field dependences of magnetization, $M(H)$, dependences for all samples at 5 and 300 K. The magnetization isotherms display a ferromagnetic behavior and reach the saturation at low temperatures above 0.4 T. The magnetization decreases with reducing $< d >$. The magnetic moment values observed in nanoparticles studied are close to the reported values [8, 9]. The field dependences of magnetization at 1 T and 5 K correspond to uniform ferromagnet having the magnetic moments of 3.4, 3.2 and 3.1 μ_B/Mn for the S1, S2 and S3 samples, respectively, which are noticeably smaller than the value of moment equal to 3.7 μ_B/Mn taking into account the presence of about 30% Mn^{4+} ions in the samples studied. It can be supposed to be attributed to the presence of non-collinear interface layers between grains for the smaller size particles.

Table 2

The parameters obtained from fitting to the Curie–Weiss law

Parameters	S1	S2	S3
H = 0.05 T			
χ_0 [emu/mol]	–0.0233	–0.0276	–0.016
C [emuK/mol]	4.98	4.28	3.62
θ [K]	354	356	355
n_{eff} [μ_B]	6.3	5.9	5.4
T_C [K]	354	356	354
H = 0.3 T			
χ_0 [emu/mol]	–0.0099	–0.0333	–0.0215
C [emuK/mol]	4.29	4.62	3.87
θ [K]	354	357	355
n_{eff} [μ_B]	5.86	6.08	5.57
T_C [K]	355	357	355
H = 0.5 T			
χ_0 [emu/mol]	–0.0185	–0.0086	–
C [emuK/mol]	4.43	4.03	–
θ [K]	354	356	–
n_{eff} [μ_B]	5.95	5.68	–
T_C [K]	356	358	–

Figure 6 shows that at $T < T_C$ in small fields we have usual magnetic reversal of domains with a susceptibility, where N is the demagnetizing factor of the sample. In fields of $H > 0.2$ T, the basic contribution to increasing magnetization is connected with

reorientation of local spin along magnetic field. In this field range, the thermodynamic behavior typical for electronic spin system with the double exchange is realized.

The measurements of hysteresis loops in field ±1 T show that a coercive field (H_{coerc}) is small for all nanopowders. A coercivity at T = 4.2 K increases from 0.001 to 0.0025 T with decreasing $< d >$ from 88 to 32 nm. A small value of coercive field indicates a very weak anisotropy energy and testifies on soft ferromagnetic behavior of the samples studied. As known, a multidomain particles have such low coercive fields. The remanent magnetization (M_{rem}) also changes slightly with changing $< d >$.

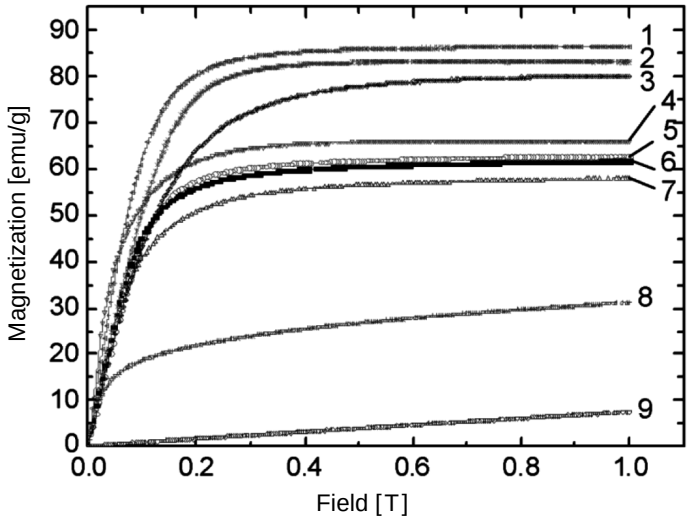

Fig. 6. Comparison of $M(H)$ dependences at 5 K for S1, S2 and S3 (curves 1–3, respectively), at T = 300 K for ceramic, S1, S2 and S3 (curves 4, 5, 6 and 7, respectively) and at 351 and 373 K for S1 (curves 8–9, respectively)

Rys. 6. Porównanie zależności $M(H)$ w T = 5 K dla próbek S1, S2 i S3 (odpowiednio: krzywe 1–3), w T = 300 K dla ceramiki, S1, S2 i S3 (odpowiednio: krzywe 4, 5, 6 i 7) i w T = 351 i 373 K dla S1(odpowiednio: krzywe 8 i 9)

To exclude the influence of magnetic dipole interactions in weak fields (demagnetizing field), the Arrot's method [27] was used to describe the temperature behavior of spontaneous magnetization in strong fields near T_C.

In Figure 7, the experimental Arrot's curves for sample PS3 near the phase transition are presented. Similar curves were obtained for S1 and S2. The temperature dependence of spontaneous magnetization was determined by linear fitting of the experimental data to Arrot's curves

$$M^2(H,T) = A + B\frac{H}{M(H,T)} \tag{3}$$

where A and B are the fitting parameters. Knowing the A factor, it is possible to find spontaneous magnetization, $M_0(T)$, as $M_0(T) = \sqrt{A}$, as well as the field dependence of spontaneous magnetization, $M_0(H)$, without taking into account of influence of domain structure.

The left inset to Fig. 7 shows the experimental field dependences of magnetization (points) and corresponding interpolation curves $M(H, T)$ (lines). Both Figure 6 and the right inset to Fig. 7, where the temperature variation of the spontaneous magnetic moment for the samples with various grain sizes is depicted, confirm that the magnetic moment decreases with decreasing particles size. It may be due to the surface effect, since in FM and AFM oxides with the particle size less than 100 nm the local order of atoms situated in the surface layer can differ considerably from that of the interior atoms [9, 14, 16]. An outer shell of particles will contain most of the oxygen vacancies and faults in the crystallographic structure that leads to magnetically disordered state. The atom disorder affecting the magnetic interactions can lead to a canting of the surface spins, or to the state when the outer layer has no net moment.

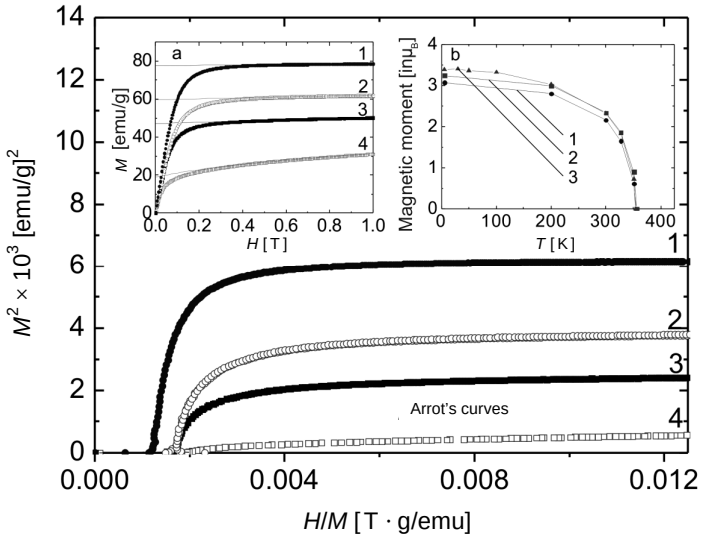

Fig. 7. Experimental Arrot's curves for samples S3 at temperatures of 200, 300, 327 and 351 K (curves 1–4, respectively). Left inset: experimental field dependences of magnetization (points) and corresponding interpolation curves $M(H,T)$ (lines). Right inset: the variation of the spontaneous magnetic moment with grain sizes for S3, S2 and S1 samples (curve 1, 2 and 3, respectively)

Rys. 7. Eksperymentalne krzywe Arrota dla próbki S3 w temperaturach 200, 300, 327 i 351 K (odpowiednio: krzywe 1–4). Lewa wstawka: eksperymentalne zależności namagnesowania od pola (punkty) i odpowiadające im krzywe dopasowania $M(H,T)$ (linie). Prawa wstawka: zmiana spontanicznego momentu magnetycznego w zależności od rozmiarów ziaren dla próbek S3, S2 i S1 (odpowiednio: krzywe 1, 2 i 3)

Comparison of experimental and calculated temperature dependences of the spontaneous magnetic moment for the S2 sample near the phase transition shows that the spontaneous magnetization both in magnetic field and without field is well described in the frame of the double exchange model.

3.1.2. Magnetocaloric effect

In this paper, the magnetocaloric effect (MCE) characterazing the magnetic entropy (ΔS_M) change produced by changes of the magnetic field applied to the system was calculated from initial magnetization curves.

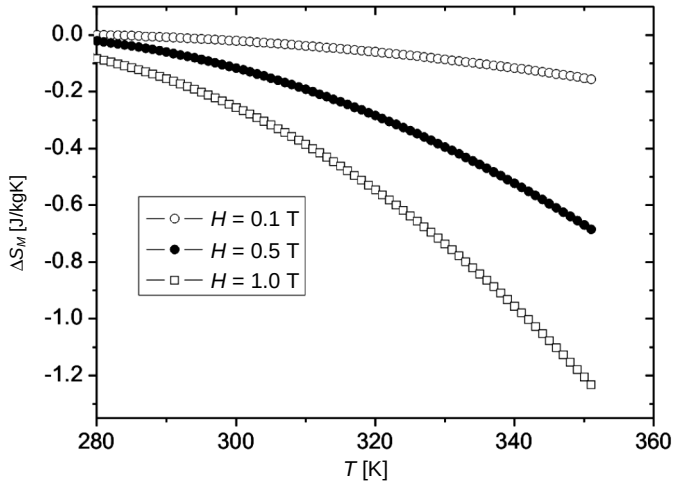

Fig. 8. Temperature dependences of entropy ΔS_M at various magnetic fields for the S3 sample
Rys. 8. Temperaturowe zależności entropii ΔS_M w różnych polach magnetycznych dla próbki S3

Using the Arrot curves (see the lines in Fig. 7) the $M(H)$ dependences and spontaneous magnetization M_0 at $H = 0$ were obtained. For above temperatures we have used the spline interpolation to find the $M(H, T)$ dependence. The temperature dependence of ΔS_M was calculated using the relation

$$\Delta S_M(T,H) = \int_0^H \left(\frac{\partial M(T,H)}{\partial T} \right)_H dH \tag{4}$$

Knowing the $M(H, T)$ dependence, we have found the derivative $\left(\frac{\partial M(T,H)}{\partial T} \right)$, and substituting it in (4) $\Delta S_M(T, H)$ was calculated.

In Figure 8, a change of the absolute ΔS_M value in the magnetoordered phase as a function of temperature at different magnetic fields for the S3 sample (d = 32 nm) is shown. Similar $\Delta S_M(T)$ dependences were obtained for other nanosize samples. The $\Delta S_M(T)$ dependences in the paramagnetic phase (above T_C) were not calculated, because the $M(H)$ were not measured. Therefore, a $\Delta S_M(T)$ peak around the magnetic phase transition was not observed. As it is seen in Fig. 8, the absolute value of magnetic entropy increases with increasing applied magnetic field. The absolute $\Delta S_M(T)$ value was found to decrease for the small particles. This behavior can be explained with the model of the nanoparticles composed of both an inner core with physical properties similar to the bulk

and an outer shell. An outer shell has disordered magnetic structure. Its role increases with reducing particle size as 1/*D* [15], where *D* is the particle size. According to the relation (4) the magnetic entropy $\Delta S_M(T)$ is depended on the magnetization value. Therefore, the decrease of absolute values of $\Delta S_M(T)$ can be explained by decreasing magnetic moment of nanopowders caused by the surface effect as the grain size decreases. The relative surface contribution, or the surface/volume of the grains ratio, increases due to the larger surface area of the small particles. Thus, the total magnetocaloric effect reduces as the particle size diminishes, since the contribution of the outer shell having the disordered magnetic state to MCE will decrease.

4. Conclusions

In this paper, magnetic measurements of nanoparticle $(La_{0.7}Sr_{0.3})_{0.9}Mn_{1.1}O_3$ manganite having an averaged grain size ranging from 32 to 88 nm have been carried out. The experimental data have shown that the nanostructuration of the grains plays an important role in the magnetism and transport of manganite studied. Its properties are strongly depended on the surface effects related to the grain sizes. The magnetization of nanopowders decreases with decreasing particle size unlike that the phase transition temperature does not show significant difference in respect to bulk counterpart. The simplest explanation of magnetic moment decrease is the existence of a noncollinear spin structure, or magnetically "dead" layer at the surface of nanoparticles as a result of the atom disorder in the surface layer. The relative surface contribution, or the surface/volume of the grains ratio, increases due to the larger surface area of the small particles, and therefore their spontaneous magnetization is diminished. This explanation agrees with a model of the nanoparticles composed of an inner core with physical properties similar to the bulk and an outer shell with oxygen vacancies, defects and etc. [16]. However, the spin disorder mechanism at the nanoparticle surface needs to be ascertained. The magnetic entropy $\Delta S_M(T)$ was shown to increase with increasing applied magnetic field and its absolute value is smaller for the small particles. The total magnetocaloric effect (MCE) reduces as the particle size diminishes, since the contribution of the outer shell having the disordered magnetic state to MCE will decrease.

The authors would like to thank to Professor A. Szytuła for discussions of results of investigations as well as to Dr S. Baran for help during X-ray diffraction measurements.

References

[1] Jin S.T., Tielfel T.H., McCormack M., Fastnacht R.A., Ramesh R., Chen L.H., Science 264 (1994), 413-415.
[2] Ramirez A.P., J. Phys.: Condens. Matter. 9 (1997), 8171-8199.
[3] Coey J.M.D., Viret M., von Molnar S., Advances in Physics 48 (1999), 167-293.
[4] Spasojevic V., Markovic D., Kusigerski V., Antic B., Boskovic S., Mitric M., Vlajic M., Krstic V., Matovic B., J. Alloys and Comp. 442 (2007), 197-199.

[5] Acha C., Garbarino G., Leyva A.G., Physica B: Condens. Matter. 398 (2007), 212-214.
[6] Markovich V., Fita I., Mogilyansky D., Wisniewski A., Puzniak R., Titelman L., Vradman L., Herskowitz M., Gorodetsky G., J. Phys.: Condens. Matter. 19 (2007), 346210-346230.
[7] Rajagopal R., Mona J., Kale S.N., Bala T., Pasricha R., Poddar P., Sastry M., Prasad L.V., Kundaliya D.C., Ogale S.B., Appl. Phys. Lett. 89 (2006), 023107-023109.
[8] Duan Y.W., Kou X.L., Li J.G., Physica B: Condens. Matter. 355 (2005), 250-254.
[9] Sanchez R.D., Rivas J., Vazquez-Vazquez C., Lopez-Quintela A., Causa M.T., Tovar M., Oseroff S., Appl. Phys. Lett. 68 (1996), 134-136.
[10] Roy S., Dubenko I., Edorh D.D., Ali N., J. Appl. Phys. 96 (2004), 1202-1208.
[11] Krivoruchko V.N., Konstantinova T., Mazur A., Prokhorov A., Varyukhin V., J. Magn. Magn. Mater. 300 (2006), e122-e125.
[12] Bibes M., Balcells L.I., Fontcuberta J., Vojcik M., Nadolski S., Jedryka E., Appl. Phys. Lett. 82 (2003), 928-930.
[13] Mahesh R., Mahendiran R., Raychaudhuri A.K., Rao C.N.R., Appl. Phys. Lett. 68 (1996), 2291-2293.
[14] Balcells L.I., Fontcuberta J., Martinez B., Obradors X., Phys. Rev. B 58 (1998), R14697-R14700.
[15] Li R.W., Xiong H., Sun J.R., Li Q.A., Wang Z.H., Zhang J., Shen B.G., J. Phys.: Condens. Matter. 13 (2001), 141-148.
[16] Lopez-Quintela M.A., Hueso L.E., Rivas J., Rivadulla F., Nanotechnology 14 (2003), 212-224.
[17] Dyakonov V., Fita I., Zubov E., Pashchenko V., Mikhaylov V., Prokopenko V., Bukhantsev Yu., Atciszewska M., Dobrowolski W., Nabialek A., Szymczak H., J. Magn. Magn. Mater. 246 (2002), 40-53.
[18] Balcells L.I., Enrich R., Mora J., Calleja A., Fontcuberta J., Obradors X., Appl. Phys. Lett. 69 (1996), 1486-1488.
[19] Pashchenko V.P., Nosanov M.I., Shemjakov A.A., *High sensitive sensor with magnetoresistive film*, Patent UA 69798 A (Bulletin 9, 2004).
[20] Pankhurst Q.A., Connolly J., Jones S.K., Dobson L., J. Phys. D 36 (2000), R167-R181.
[21] Rodriguez-Carvajal J., Physica B 192 (1993), 55.
[22] Brunauer S., Emmett P.H., Teller E., J. Am. Chem. Soc. 60 (1938), 309-315.
[23] Cullity B.D., *Elements of X-ray Diffraction*, Addison-Wesley, Reading, MA, 1078.
[24] Rasberry S.D., Bureau of Standards Certificate – Standard Reference Material 640b, 1987.
[25] Raveau B., Zhao Y.M., Martin C., Hervieu M., Maignan A., J. Solid State Chem. 149 (2000), 203-207.
[26] De Brion S., Ciorcas F., Chouteau G., Lejay P., Radaelli P., Chaillout C., Phys. Rev. B 59 (1999), 1304-1310.
[27] Arrot A., Phys. Rev. 108 (1957), 1394-1396.